arXiv:1302.0396v1 [cond-mat.str-el] 2 Feb 2013

Tailoring the electronic texture of a topological insulator via its surface orientation

Lucas Barreto,[1] Wendell Simoes e Silva,[2, 1] Malthe Stensgaard,[1] Søren Ulstrup,[1]
Xie-Gang Zhu,[1] Marco Bianchi,[1] Maciej Dendzik,[3, 1] and Philip Hofmann[1, 4]
[1]*Department of Physics and Astronomy, Interdisciplinary Nanoscience Center (iNANO), Aarhus University, 8000 Aarhus C, Denmark*
[2]*Departamento de Física, Universidade Federal de Minas Gerais, 30123-970, Belo Horizonte, Brazil*
[3]*Centre for Nanometer-Scale Science and Advanced Materials (NANOSAM), Smoluchowski Institute of Physics, Jagiellonian University, Reymonta 4, 30-059 Kraków, Poland*
[4]*email: philip@phys.au.dk*

(Dated: February 5, 2013)

Three dimensional topological insulator crystals consist of an insulating bulk enclosed by metallic surfaces, and detailed theoretical predictions about the surface state band topology and spin texture are available [1–7]. While several topological insulator materials are currently known, the existence and topology of these metallic states have only ever been probed for one particular surface orientation of a given material. For most topological insulators, such as $\mathrm{Bi}_{1-x}\mathrm{Sb}_x$ and $\mathrm{Bi}_2\mathrm{Se}_3$, this surface is the closed-packed (111) surface and it supports one topologically guaranteed surface state Dirac cone. Here we experimentally realise a non closed-packed surface of a topological insulator, $\mathrm{Bi}_{1-x}\mathrm{Sb}_x(110)$, and probe the surface state topology by angle-resolved photoemission. As expected, this surface also supports metallic states but the change in surface orientation drastically modifies the band topology, leading to three Dirac cones instead of one, in excellent agreement with the theoretical predictions [5] but in contrast to any other experimentally studied TI surface. This illustrates the possibility to tailor the basic topological properties of the surface via its crystallographic direction. Here it introduces a valley degree of freedom not previously achieved for topological insulator systems.

PACS numbers:

For the topological insulator (TI) surfaces studied so far, the predicted Fermi contour consists of an odd number of Dirac cones around the Brillouin zone centre $\bar{\Gamma}$ (see e.g. Refs. [8–12]) but more complex scenarios with Dirac cones around three translation invariant momenta (TRIMs) have been predicted for non-(111) surfaces of $\mathrm{Bi}_{1-x}\mathrm{Sb}_x$ [5] and for $\mathrm{SmB}_6(001)$ [13]. The possibility of such a scenario is closely linked to the bulk electronic structure of a TI: If the bulk parity inversion only takes place at the Brillouin zone centre Γ, this leads to an odd number of closed Fermi contours around the surface Brillouin zone centre $\bar{\Gamma}$ for every possible surface orientation, but if the bulk parity inversion happens at another bulk TRIM, one should be able to change the surface state topology by choosing different surface orientations. Candidates for TI materials allowing this are $\mathrm{Bi}_{1-x}\mathrm{Sb}_x$ (parity inversion at every bulk TRIM except L [5]), $\mathrm{PbBi}_2\mathrm{Te}_4$ (parity inversion at Z [11]) and SbB_6 (parity inversion at X [13]).

So far, surface state topology investigations by angle-resolved photoemission spectroscopy (ARPES) have only been performed for surfaces with a topologically predicted single Dirac cone around $\bar{\Gamma}$. Indeed, only one surface orientation for a given TI has so far been probed, such that even the basic expectation of a bulk material completely enclosed by metallic surfaces still needs to be verified. Experiments for other surface orientations are lacking due to the difficulty of preparing such surfaces. Feasible methods for preparing TI surfaces are cleaving [8, 9], a combination of cutting, polishing and *in situ* cleaning, as well as epitaxial growth [14–16]. While cleaving and epitaxial growth have so far only been used to prepare the very stable (111) surface (except for the cubic HgTe(001) [16]), cutting and *in situ* cleaning could in principle give any desired surface direction, but the approach is hindered by the small size of crystals, their strong anisotropy and the high likelihood to off-set the delicate stoichiometry near the surface during the *in situ* cleaning process.

Here we show that an epitaxial film of the topological insulator $\mathrm{Bi}_{1-x}\mathrm{Sb}_x$ can be grown in the (110) orientation by evaporating a mixture of Bi and Sb on a Bi(110) surface. Since x is quite small in the TI phase ($0.09 < x < 0.18$), the lattice mismatch between the Bi substrate and the film is so small [17] that the growth is quasi-homoepitaxial, resulting in a high-quality $\mathrm{Bi}_{1-x}\mathrm{Sb}_x(110)$ film. Fig. 1(a) shows the Fermi contour for a film of $\mathrm{Bi}_{0.86}\mathrm{Sb}_{0.14}(110)$ measured by ARPES (i.e. the photoemission intensity at the Fermi level) and it is immediately obvious that for this surface three TRIMs are enclosed by Fermi contours: $\bar{\Gamma}, \bar{M}$ and $\bar{X}_1$, in sharp contrast to the (111) surface of this TI where only the $\bar{\Gamma}$ point is enclosed by an odd number of Fermi contours.

Before discussing the experimental results in more detail, we briefly review the theoretical predictions for the $\mathrm{Bi}_{1-x}\mathrm{Sb}_x$ surfaces by Teo, Fu and Kane [5]. Their approach and its results are illustrated in Fig. 1(c)-(e). The parity invariants δ for the eight bulk time-reversal invariant momenta (TRIMs) Γ_i in $\mathrm{Bi}_{1-x}\mathrm{Sb}_x$ are all found to be -1, except for the bulk L point where $\delta(L) = 1$ for

$Bi_{1-x}Sb_x$ with ($x > 0.09$) and $\delta(L) = -1$ otherwise. The surface fermion parity π for each surface TRIM determines the topology of the surface Fermi contour. It can be calculated from a projection of the bulk parity invariants using the relation $\pi(\Lambda_a) = (-1)^{n_b}\delta(\Gamma_i)\delta(\Gamma_j)$, where n_b is the number of occupied, spin-degenerate bulk bands, i.e. 5 for $Bi_{1-x}Sb_x$. This procedure is illustrated in Fig. 1(c) together with the bulk and surface Brillouin zones. The predicted surface fermion parity values for the surface TRIMs of the (111) and (110) surfaces in the TI state ($x > 0.09$) are also shown. The surface fermion parity values for the surface TRIMs immediately give the topological prediction for the Fermi contour: the TRIM should be enclosed by an odd number of contours for $\pi = -1$ and by an even or no contour for $\pi = 1$. The topologically expected closed contours are marked by blue circles. $Bi_{1-x}Sb_x$(111) shows one such contour in the surface Brillouin zone whereas $Bi_{1-x}Sb_x$(110) has three.

The topological predictions for $Bi_{1-x}Sb_x$(110) and Bi(110) are compared in Fig. 1(d) and (e). The quantum phase transition to a TI at $x = 0.09$ changes the bulk Fermion parity for the L point from -1 to 1 and this leads to a surface fermion parity change at $\bar{X}_2$: For $Bi_{1-x}Sb_x$(110) one expects to find an odd number of Fermi level crossings between $\bar{X}_2$ and any other TRIM whereas there would be an even number for Bi(110). Note that such a rich surface state topology would not be expected for a non-(111) surface of most other topological insulators (e.g. Bi_2Se_3) because there the bulk parity inversion happens only at the Γ point ($\delta(\Gamma) = -1$), which, combined with the even n_b, leads to merely an odd number of closed contours around the $\bar{\Gamma}$ point of the surface, as illustrated for Bi_2Se_3(110) in Fig. 1(f).

The measured Fermi surfaces for Bi(110) and $Bi_{0.86}Sb_{0.14}$(110) are shown in Fig. 1(a) and (b), respectively. They are, at first glance, very similar to each other and to published results for Bi(110) [18, 19]. The dominating features are topologically required closed contours around the $\bar{\Gamma}$, $\bar{M}$ and $\bar{X}_1$ points as well as a small electron pocket on the $\bar{X}_1 - \bar{M}$ line. This electron pocket does not encircle any TRIM and is irrelevant for the surface state topology, but in order to facilitate the comparison between the topological predictions and the data, it has been included as a yellow feature in Fig. 1(d),(e). The topological prediction for Bi(110) also requires the existence of a closed Fermi contour around $\bar{X}_2$, but this is not clearly confirmed by the data in this overview scan. In any event, such predictions do not necessarily have to be fulfilled for a semimetal because the topologically required parity changes between surface TRIMs could also be accomplished by the bulk states crossing the Fermi surface. Such projected bulk Fermi surface elements are found near the $\bar{X}_1$ and $\bar{X}_2$ points on Bi(110). They are indicated by the red areas in Fig. 1(e).

The topological quantum phase transition from Bi to $Bi_{1-x}Sb_x$ should be reflected in a change of the surface state dispersion around the $\bar{X}_2$ point. This is consistent with the observed change between the Fermi surface maps of Fig. 1(a) and (b): While the photoemission intensity at the Fermi level near $\bar{X}_2$ is an elongated stripe in the $\bar{\Gamma} - \bar{X}_2$ direction for Bi(110), this stripe is split into two features on either side of $\bar{X}_2$ for $Bi_{0.86}Sb_{0.14}$. This situation near $\bar{X}_2$ is further explored by a high-resolution scan along $\bar{\Gamma} - \bar{X}_2$ for both $Bi_{0.86}Sb_{0.14}$(110) and Bi(110) in Fig. 2. The surface state dispersion in this direction is quite different in the two cases: Both surfaces share the hole pocket around $\bar{\Gamma}$ but whereas the band forming this pocket disappears into the projected band states for $Bi_{0.86}Sb_{0.14}$(110), its dispersion reaches a binding energy maximum for Bi(110) before it disperses back towards the Fermi level. It only merges with the bulk bands in the immediate vicinity of the $\bar{X}_2$ point. For $Bi_{0.86}Sb_{0.14}$(110), on the other hand, there is no state observable at $\bar{X}_2$ but a shallow electron pocket very close to this point.

These differences in the band structure bring the expected topology change about. For Bi(110), one would expect the $\bar{X}_2$ point to be encircled by an odd number of Fermi contours. Experimentally, the situation is somewhat unclear because it cannot be determined if the surface state band barely crosses the Fermi level on both sides of $\bar{X}_2$, forming a small hole pocket around the point, or if it stays occupied. In any case, this is not important because one would not necessarily expect the topological predictions to be strictly fulfilled to for a semimetal surface. Any required change of parity could be brought about by the bulk band continuum near $\bar{X}_2$. For $Bi_{0.86}Sb_{0.14}$(110), on the other hand, the topological predictions should be strictly followed. In contrast to the situation for Bi(110), $\bar{X}_2$ should not be encircled by a closed Fermi contour and it clearly is not: the shallow electron pocket marked by a yellow line is close to the $\bar{X}_2$ point but it does not encircle it. Indeed, the electron pockets on either side of $\bar{X}_2$ can clearly be seen in the Fermi surface scan of Fig. 1(a).

A final topological prediction for $Bi_{0.86}Sb_{0.14}$ is the existence of a closed Fermi contour around $\bar{X}_1$. This can already be seen in Fig. 1(a) but is shown more clearly by a detailed inspection of the band structure around this TRIM in Fig. 3. The high-resolution Fermi contour in Fig. 3(a) already shows a closed contour around $\bar{X}_1$ in the immediate vicinity of the two electron pockets along $\bar{X}_1 - \bar{M}$. Scans around $\bar{X}_1$ towards $\bar{M}$ and $\bar{\Gamma}$ reveal that this feature is another electron pocket. In fact, the band giving rise to it merges with the lower Rashba-split surface state bands originating from $\bar{M}$ and $\bar{\Gamma}$ to form a Dirac point at $\bar{X}_1$ but this Dirac point is situated in the projected valence band. This situation and the shape of the Fermi contour around $\bar{X}_1$ is similar to the situation on Sb(110), i.e. the case of $x = 1$ [20].

The entire Fermi contour of $Bi_{0.86}Sb_{0.14}$(110) is thus in excellent agreement with the theoretical predictions

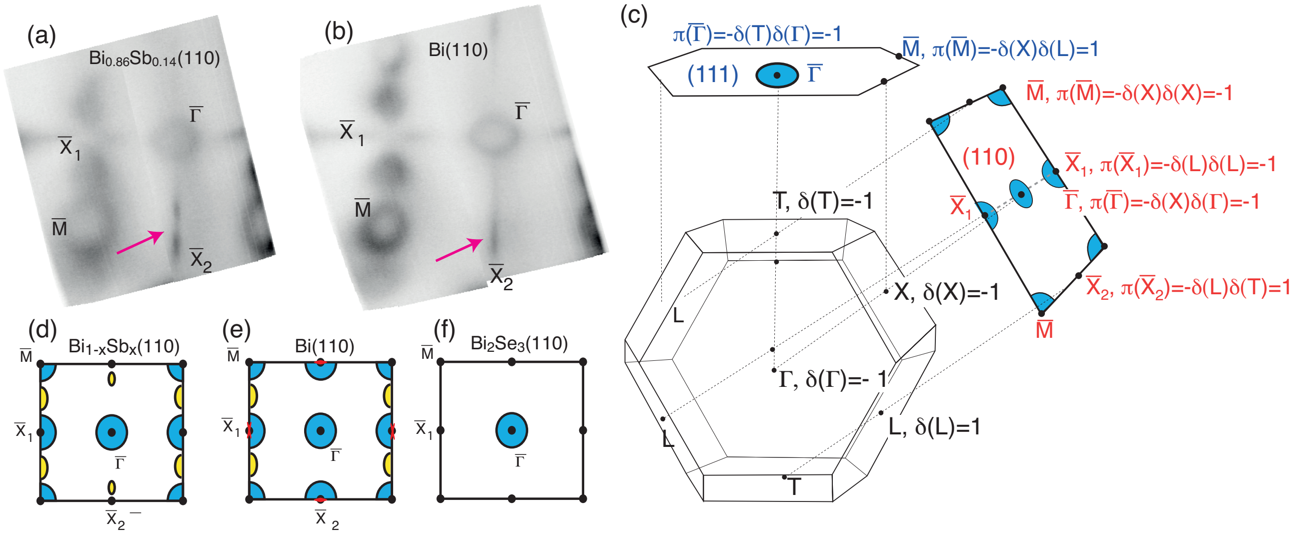

FIG. 1: (a) and (b) Photoemission intensity at the Fermi energy for $Bi_{0.86}Sb_{0.14}(110)$ and Bi(110), respectively. Dark corresponds to high intensity. The spectroscopic signature of the topological quantum phase transition is expected close to the $\bar{X}_2$ point where a splitting of a Fermi surface feature is observed (marked by arrows). (c) Projection of the bulk parity invariants δ onto the (111) and (110) surfaces of $Bi_{1-x}Sb_x$, resulting in the surface fermion parity values π for the time-reversal invariant momenta (TRIMs). The black dots mark the positions of the time-reversal invariant momenta (TRIMs) in the surface Brillouin zone. The blue areas surrounding TRIMs denote an odd number of closed Fermi contours around the TRIM. (d) - (f) Topological prediction for the surface electronic structure of the (110) surfaces of $Bi_{1-x}Sb_x$ ($x > 0.09$), Bi and Bi_2Se_3, respectively. The yellow contours are additional but topologically insignificant Fermi contour features found in the experiment. The small red features in (e) correspond to the projected bulk Fermi surface.

for this surface. It is also substantially more complex than that of $Bi_{1-x}Sb_x(111)$ or the predictions of the non-(111) surfaces of Bi_2Se_3-type topological insulators. Indeed, this illustrates the design possibilities when exploiting the surface orientation of a topological insulator. The example shown here is particularly interesting because it adds a valley degree of freedom to the topological Dirac fermions, something that is currently attracting great attention in the case of graphene [21]. It should also be possible to use the same strategy for the construction of quasi one-dimensional surface states on three-dimensional topological insulators, as already found for the vicinal parent surface Bi(114) [22].

METHODS

Experiments were performed at the SGM-3 beamline of the synchrotron radiation source ASTRID [23]. Thin films of $Bi_{1-x}Sb_x(110)$ were grown *in situ* on a Bi(110) substrate by simultaneous evaporation of Bi and Sb from an e-beam source. The Bi(110) surface had previously been cleaned by cycles of Ne ion sputtering and annealing. Data were taken for different film thicknesses and compositions. The data shown here were obtained from a film with a thickness of approximately 25 double layers and $x = 0.14$ (here the term double layer is used to group the first and second layer of the A7(110) surface. These are almost at the same height [24–26]). The growth rate and chemical composition of the film were determined by inspecting the shallow Sb 4d and Bi 5d core levels, as in Ref. 15. The energy and angular resolution for ARPES measurements were better than 20 meV and 0.2°, respectively. The photon energy was 28.5 eV for the data shown in Fig. 1 and 18 eV otherwise. Data were collected for many different photon energies between 14 eV and 32 eV in order to make sure that the features discussed above as surface states are in fact surface states, i.e. that their dispersion does not depend on the photon energy. The sample temperature during the measurements was 80 K. The bulk Fermi surface projections and band structure surface projection were calculated using the tight-binding parameters of Liu and Allen [27]. For the alloy, the parameters were interpolated following the method in Ref. 5. The calculation of the surface band structure follows the transfer matrix method used in Ref. 5 but employs a Green's function method to calculate the spectral function for a semi-infinite crystal [28].

ACKNOWLEDGEMENTS

We gratefully acknowledge financial support from the Carlsberg foundation, the VILLUM foundation, The Danish Council for Independent Research / Technology and Production Sciences. WSS acknowledges support by

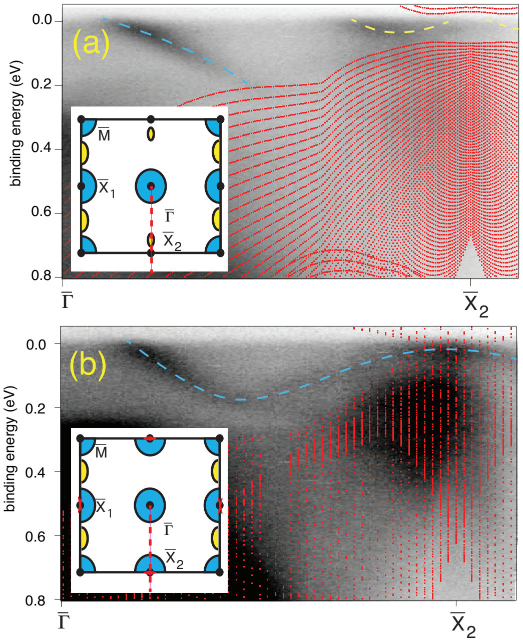

FIG. 2: Detailed electronic structure along the $\bar{\Gamma}-\bar{X}_2$ line for (a) $Bi_{0.86}Sb_{0.14}(110)$ and (b) Bi(110). Dispersing surface states are marked by dashed coloured lines as a guide to the eye. The red dots denote the projected bulk band structure. The inset shows the surface Brillouin zone with the topological predictions in blue and additional experimentally found Fermi contours in yellow. The magenta lines in the inset mark the scan direction.

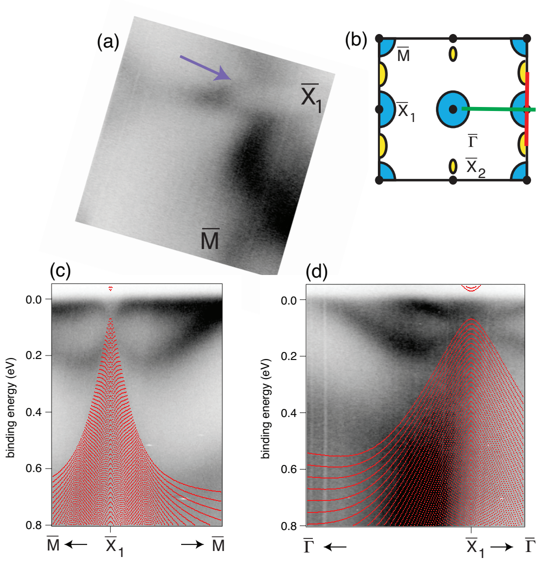

FIG. 3: Detailed electronic structure around the $\bar{X}_1$ point of $Bi_{0.86}Sb_{0.14}(110)$, confirming the existence of a closed Fermi contour around this point. (a) Photoemission intensity at the Fermi level. The arrow marks the closed contour. (b) Sketch of the surface Brillouin zone with the scan directions marked by a green and a magenta line. For the colour coding of the schematically indicated Fermi surface features, see caption of Fig. 1. (c) Band structure around $\bar{X}_1$ towards the $\bar{M}$ points (magenta line in (b)). (d) Band structure around $\bar{X}_1$ towards the $\bar{\Gamma}$ points (green line in (b)). The closed Fermi contour around $\bar{X}_1$ is found to be an electron pocket. A Dirac point is formed at $\bar{X}_1$, but it lies inside the projected continuum of the bulk valence band. The projected band structure is outlined by the red dots.

the the Brazilian funding agencies CNPq and CAPES.

[1] Liang Fu and C. L. Kane. Topological insulators with inversion symmetry. *Physical Review B*, **76**, 045302, 2007.

[2] Liang Fu, C. L. Kane, and E. J. Mele. Topological Insulators in Three Dimensions. *Physical Review Letters*, **98**, 106803, 2007.

[3] J. E. Moore and L. Balents. Topological invariants of time-reversal-invariant band structures. *Phys. Rev. B*, **75**, 121306, 2007.

[4] Shuichi Murakami. Phase transition between the quantum spin Hall and insulator phases in 3D: emergence of a topological gapless phase. *New Journal of Physics*, **9**, 356, 2007.

[5] Jeffrey C. Y. Teo, Liang Fu, and C. L. Kane. Surface states and topological invariants in three-dimensional topological insulators: Application to Bi_{1-x} Sb_x. *Physical Review B*, **78**, 045426, 2008.

[6] Xi Dai, Taylor L. Hughes, Xiao-Liang Qi, Zhong Fang, and Shou-Cheng Zhang. Helical edge and surface states in HgTe quantum wells and bulk insulators. *Phys. Rev. B*, **77**, 125319, 2008.

[7] Haijun Zhang, Chao-Xing Liu, Xiao-Liang Qi, Xi Dai, Zhong Fang, and Shou-Cheng Zhang. Topological insulators in Bi_2Se_3, Bi_2Te_3 and Sb_2Te_3 with a single Dirac cone on the surface. *Nature Physics*, **5**, 438–442, 06 2009.

[8] D. Hsieh, D. Qian, L. Wray, Y. Xia, Y. S. Hor, R. J. Cava, and M. Z. Hasan. A topological Dirac insulator in a quantum spin Hall phase. *Nature*, **452**, 970–974, 2008.

[9] Y. Xia, D. Qian, D. Hsieh, L. Wray, A. Pal, H. Lin, A. Bansil, D. Grauer, Y. S. Hor, R. J. Cava, and M. Z. Hasan. Observation of a large-gap topological-insulator class with a single Dirac cone on the surface. *Nature Physics*, **5**, 398–402, 2009.

[10] Y. L. Chen, J. G. Analytis, J. H. Chu, Z. K. Liu, S. K. Mo, X. L. Qi, H. J. Zhang, D. H. Lu, X. Dai, Z. Fang, S. C. Zhang, I. R. Fisher, Z. Hussain, and Z. X. Shen. Experimental Realization of a Three-Dimensional Topological Insulator, Bi_2Te_3. *Science*, **325**, 178–181, 7 2009.

[11] K. Kuroda, H. Miyahara, M. Ye, S. V. Eremeev, Yu. M. Koroteev, E. E. Krasovskii, E. V. Chulkov, S. Hiramoto, C. Moriyoshi, Y. Kuroiwa, K. Miyamoto, T. Okuda, M. Arita, K. Shimada, H. Namatame, M. Taniguchi, Y. Ueda, and A. Kimura. Experimental Verification of $PbBi_2Te_4$ as a 3D Topological Insulator. *Phys. Rev. Lett.*, **108**, 206803, May 2012.

[12] M. Neupane, S.-Y. Xu, L. A. Wray, A. Petersen, R. Shankar, N. Alidoust, Chang Liu, A. Fedorov, H. Ji, J. M. Allred, Y. S. Hor, T.-R. Chang, H.-T. Jeng, H. Lin, A. Bansil, R. J. Cava, and M. Z. Hasan. Topological surface states and Dirac point tuning in ternary topological insulators. *Phys. Rev. B*, **85**, 235406, Jun 2012.

[13] Feng Lu, JianZhou Zhao, Hongming Weng, Zhong Fang, and Xi Dai. Correlated Topological Insulators with Mixed Valence. *arXiv:1211.5863v1*, , 2012.

[14] Tong Zhang, Peng Cheng, Xi Chen, Jin-Feng Jia, Xucun Ma, Ke He, Lili Wang, Haijun Zhang, Xi Dai, Zhong Fang, Xincheng Xie, and Qi-Kun Xue. Experimental Demonstration of Topological Surface States Protected by Time-Reversal Symmetry. *Physical Review Letters*, **103**, 266803, 2009.

[15] T. Hirahara, Y. Sakamoto, Y. Saisyu, H. Miyazaki, S. Kimura, T. Okuda, I. Matsuda, S. Murakami, and S. Hasegawa. Topological metal at the surface of an ultrathin Bi_{1-x} Sb_x alloy film. *Phys. Rev. B*, **81**, 165422, Apr 2010.

[16] C. Brüne, C. X. Liu, E. G. Novik, E. M. Hankiewicz, H. Buhmann, Y. L. Chen, X. L. Qi, Z. X. Shen, S. C. Zhang, and L. W. Molenkamp. Quantum Hall Effect from the Topological Surface States of Strained Bulk HgTe. *Phys. Rev. Lett.*, **106**, 126803, 2011.

[17] H. Berger, B. Christ, and J. Troschke. Lattice Parameter Study in the Bi1–xSbx Solid-solution System. *Crystal Research and Technology*, **17**, 1233–1239, 1982.

[18] S. Agergaard, C. Søndergaard, H. Li, M. B. Nielsen, S. V. Hoffmann, Z. Li, and Ph. Hofmann. The effect of reduced dimensionality on a semimetal: The electronic structure of the Bi(110) surface. *New Journal of Physics*, **3**, 15.1–15.10, 2001.

[19] J. I. Pascual, G. Bihlmayer, Y. M. Koroteev, H. P. Rust, G. Ceballos, M. Hansmann, K. Horn, E. V. Chulkov, S. Blugel, P. M. Echenique, and Ph. Hofmann. Role of spin in quasiparticle interference. *Physical Review Letters*, **93**, 196802, 2004.

[20] Marco Bianchi, Dandan Guan, Anna Stróżecka, Celia H. Voetmann, Shining Bao, Jose Ignacio Pascual, Asier Eiguren, and Philip Hofmann. Surface states on a topologically nontrivial semimetal: The case of Sb(110). *Phys. Rev. B*, **85**, 155431, Apr 2012.

[21] A. Rycerz, J. Tworzydlo, and C. W. J. Beenakker. Valley filter and valley valve in graphene. *Nature Physics*, **3**, 172–175, 03 2007.

[22] J. W. Wells, J. H. Dil, F. Meier, J. Lobo-Checa, V. N. Petrov, J. Osterwalder, M. M. Ugeda, I. Fernandez-Torrente, J. I. Pascual, E. D. L. Rienks, M. F. Jensen, and Ph. Hofmann. Nondegenerate Metallic States on Bi(114): A One-Dimensional Topological Metal. *Physical Review Letters*, **102**, 096802, 2009.

[23] S. V. Hoffmann, C. Søndergaard, C. Schultz, Z. Li, and Ph. Hofmann. An undulator-based spherical grating monochromator beamline for angle-resolved photoemission spectroscopy. *Nuclear Instruments and Methods in Physics Research, A*, **523**, 441, 2004.

[24] F. Jona. Low-energy electron diffraction study of surfaces of antimony and bismuth. *Surface Science*, **8**, 57–76, 1967.

[25] Ph. Hofmann. The surfaces of bismuth: Structural and electronic properties. *Progress in Surface Science*, **81**, 191–245, 2006.

[26] J. Sun, A. Mikkelsen, M. Fuglsang Jensen, Y. M. Koroteev, G. Bihlmayer, E. V. Chulkov, D. L. Adams, Ph. Hofmann, and K. Pohl. Structural determination of the Bi(110) semimetal surface by leed analysis and ab initio calculations. *Physical Review B*, **74**, 245406, 2006.

[27] Yi Liu and Roland E. Allen. Electronic structure of the semimetals Bi and Sb. *Physical Review B*, **52**, 1566, 1995.

[28] Eugene J. Mele and J. D. Joannopoulos. Electronic states at unrelaxed and relaxed GaAs (110) surfaces. *Phys. Rev. B*, **17**, 1816–1827, Feb 1978.